Triton and alpha-particle production in neutron-induced reactions on carbon at E_n=42.5, 62.7, and 72.8 MeV

I. Slypen, V. Corcalciuc, and J. P. Meulders
Institut de Physique Nucléaire, Université Catholique de Louvain, Chemin du Cyclotron 2, B-1348 Louvain-la-Neuve, Belgium

M. B. Chadwick*
University of California, Nuclear Data Group, L412, Lawrence Livermore National Laboratory, Livermore, California 94550
(Received 26 May 1995)

Double-differential cross sections for fast neutron-induced triton and alpha-particle production on carbon are reported at three incident neutron energies: 42.5, 62.7, and 72.8 MeV, complementing our previous results for proton and deuteron emissions. Angular distributions were measured at laboratory angles between 20° and 160° in steps of 10°. Procedures for data taking and data reduction are described. Results for double-differential, energy-differential, and total cross sections are presented. The measurements are compared to existing data and to nuclear model calculations which include preequilibrium and equilibrium decay mechanisms.

PACS number(s): 25.40.Hs, 24.60.Gv, 28.20.−v

I. INTRODUCTION

Experimental measurements of charged-particle production for neutron-induced reactions on carbon in the incident energy range 30–80 MeV are rather scarce [2]. Subramanian *et al*. at UC Davis measured emission spectra of hydrogen and helium isotopes at 27, 40, and 61 MeV [3]. In a recent paper our results for proton and deuteron emission at incident neutron energies of 42.5, 62.7, and 72.8 MeV, respectively, were given [1]. In the present paper we report measurements of double-differential triton and α-particle production cross sections from carbon at these same incident neutron energies.

Neutron reactions on carbon in the above energy range are of interest in both basic and applied physics. Experimental measurements enable nuclear reaction theories and models to be tested and developed for light nuclei, which present a particular challenge due to their wide-spaced low-lying nuclear levels and their nonstatistical properties. An accurate understanding of charged-particle production cross sections from carbon is also important for determining energy deposition from neutrons in radiotherapy, and in intermediate-energy accelerators that are currently being considered for applications such as the transmutation of long-lived nuclear waste into shorter-lived products [4]. These cross sections are also needed for determining the response of neutron detectors [5].

In Sec. II the experimental setup and data reduction procedures are briefly presented. Experimental results are shown in Sec. III. In Sec. IV we describe nuclear model calculations which include direct, preequilibrium, and equilibrium reaction mechanisms, and in Sec. V we compare our measurements with both our model predictions of double-differential and angle-integrated emission spectra and the UC Davis experimental results [3]. We also compare our results with the model calculations of Brenner and Prael [6]. Conclusions are given in Sec. VI.

II. EXPERIMENTAL METHODS

The present paper reports experimental data for triton and α-particle production in fast neutron-induced reactions on carbon and follows on from our previous publication concerning proton and deuteron production [1]. Since the experimental setup and data reduction procedures are the same as those in our previous work, only essential details are given here. For further information the reader is referred to Ref. [1] and the references therein.

The accelerated proton beam of the Louvain-la-Neuve Cyclotron CYCLONE fast neutron beam facility [7–9], focused on a 3 mm thick natural lithium target, was used to produce a quasimonoenergetic neutron beam at 0° laboratory angle [1,10]. With a 10^{-5} A proton beam, about 10^6 neutrons/s are available at the location of our reaction chamber. The neutron energy spectrum at 0° consists of a well-defined peak (with full width at half maximum of 2 MeV) containing about 50% of the neutrons, plus a flat continuum of low-energy neutrons [1].

The evacuated reaction chamber (406 mm in diameter) was coupled to the exit of the neutron collimator, and laboratory angles from 20° to 160° in steps of 10° were available for measurements.

Four charged-particle detector telescopes were used simultaneously. Each of them consisted of a ΔE detector (NE102 plastic scintillator, 0.1 mm thick, 4 cm in diameter) viewed by an XP2020 photomultiplier via a Lucite light guide, and of an E detector [CsI(Tl) crystal, 22 mm thick, 38.1 mm in diameter], viewed by an XP2262B photomultiplier. The E detector can stop 80 MeV protons. A coincidence was required between ΔE and E detectors in order to suppress an important part of the background present in such types of experiment.

An elemental carbon target (5×5 cm^2 surface and 1 mm

*Corresponding author, telephone: (505) 667 9877. Present address: Theoretical Division, MSB243, Los Alamos National Laboratory, Los Alamos, NM 87545. Electronic address: mbchadwick@lanl.gov

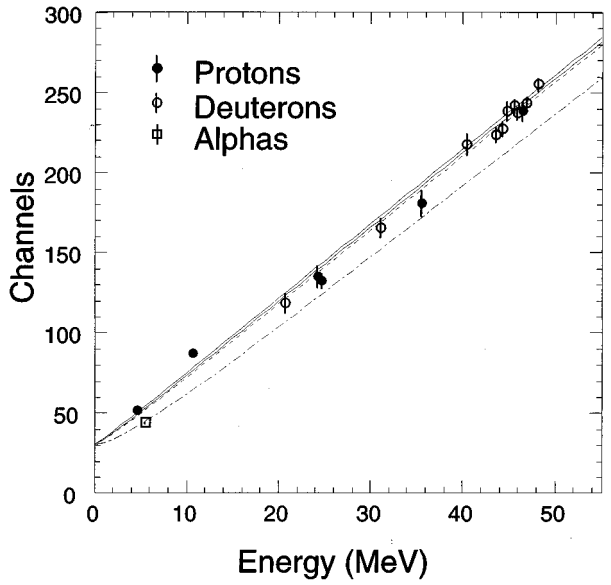

FIG. 1. Energy calibration curves for protons and deuterons (continuous lines), tritons (dashed line), and α particles (dashed-dot line) as result of a fit with a three-parameter formula of Ref. [11]. The experimental points result from H(n,p) and D(n,d) scattering on, respectively, a polypropylene and a deuterated polypropylene target. An α-source point (about 5.5 MeV) is also shown.

thick) was used. The angle of the target with the beam was chosen to minimize the thickness of the target material traversed by the charged-particle ejectiles towards the telescopes.

Bringing a direct charged-particle beam to the reaction chamber is not easy in the present neutron facility. Therefore, for the energy calibration, the protons and deuterons recoiling from a polypropylene (1 or 0.5 mm thick) and a 0.6 mm thick deuterated polypropylene target, respectively, were used. They were recorded at laboratory angles from 20° to 70° in steps of 10°, at each of the three incident neutron energies, for each of the four telescopes used. These measurements provided a reliable energy calibration for protons and deuterons. Previous experimental work on the light response of CsI crystals to the detection of a large variety of charged particles related the crystal light response to the energy of the detected charged particle by a simple three-parameter analytical formula [11,12]. Using this formula in a simultaneous fit to the proton (about seven points) and deuteron (about seven points) energy calibration points and a supplementary α-source point (at about 5.5 MeV), the three parameters were determined. Figure 1 gives an example of the resulting energy calibration. Evidently the errors on the three free parameters induce errors in the energy calibration. Therefore, the energy spectra for triton and α-particle production are reported here as histograms in steps of 3 MeV for the outgoing particle energies. Moreover, as the measured cross sections are rather small, this choice of the energy step improves the statistics in the reported spectra.

Charged-particle discrimination spectra were obtained in two ways: by using the energy information from ΔE and E detectors, and by charge integration of the CsI light output pulse [13–15]. A combined use of these two separation methods allows a good separation of the reaction products over their entire energy range as well as an efficient elimination of most of the background [1,14,15].

The beam monitoring system was realized in two ways. The incident proton beam is magnetically deflected, after passing the lithium target, into a water-cooled Faraday cup and then integrated [8,9]. Downstream of our reaction chamber, and coupled to it, is a second evacuated chamber in which a charged-particle telescope detects the H(n,p) scattered protons at 45° [1]. The agreement between these two monitoring systems was very good during the data taking.

For each charged-particle event in the telescopes, the time of flight (TOF) between a capacitive beam pickoff, located upstream of the neutron producing target, and the ΔE detector is registered and subsequently used to select only those events associated with neutrons in the main neutron peak [1,14,15].

Data were archived on workstation disks and on Exabyte tapes for an off-line analysis.

By complementary use of ΔE-E and slow vs fast components in the particle discrimination spectra, a reliable selection of the desired events was obtained [1,14,15]. Subsequently, using TOF information and knowing the flight distances and energies of the particles (from the energy calibration), a further selection was made for only those events induced by neutrons from the monoenergetic peak [14,15].

The statistics in our spectra correspond to an acquisition time of 24 h for forward and 48 h for backward angles, with about 12×10^{-6} A mean proton beam on a 3 mm thick lithium target.

Absolute cross sections were obtained by normalization to our measured H(n,p) scattering cross sections. Angular distributions for the n-p elastic scattering were measured at six laboratory angles between 20° and 70° at each incident neutron energy and for each telescope. Solid angles and thick target corrections were calculated with a Monte Carlo simulation program of the experiment [16]. The average angular opening of the collimating system for the detection of charged particle products was 2°–3° and the neutron beam energy width, for the main peak, was about 2 MeV.

In this way, for each of the telescopes, six normalization points were available covering a large energy range, and the normalization factor was obtained from their mean value. Generally the spread of these values around the mean was less than 3%. Normalization factors of the order of 2×10^{-4} for forward and 10^{-4} for backward angles were obtained.

The rather thick carbon target, the 0.1 mm thick ΔE detector used, and the energy threshold of the E detector (about 1.5 MeV) limit the registration of the low-energy charged-particle products to only fractions of the entire target thickness, and therefore the spectra should be corrected accordingly. These effects are taken into account by using the above-mentioned simulation program [1,16].

III. EXPERIMENTAL RESULTS

Using the procedures outlined above, double-differential cross sections for triton and α-particle production were obtained for three incident neutron energies corresponding to the main neutron peaks, 42.5, 62.7, and 72.8 MeV, resulting, respectively, from 45, 65, and 75 MeV incident protons on the lithium target. Figures 2–7 show, in three-dimensional

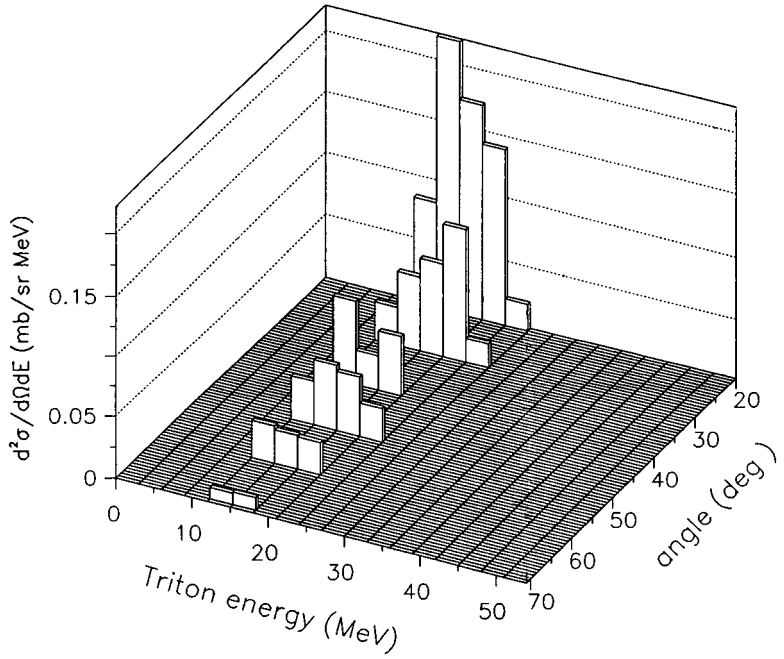

FIG. 2. Angular distributions of measured double-differential cross sections (histograms in steps of 3 MeV) for triton production at 42.5 MeV incident neutron energy.

(3D) representations, the measured energy spectra of tritons and α particles and their angular distributions, for the above-mentioned incident neutron energies. The energy spectra are represented as histograms in steps of 3 MeV. The horizontal scale gives the energy of the charged particles produced in the reaction. Low-energy cuts are about 12 MeV for both tritons and α particles. The high values of the low-energy cuts in the triton spectra are due to the rather poor separation of the low-energy tritons in the particle identification spectra. In spite of our long acquisition runs, no significant statistics could be accumulated at some laboratory angles in the backward hemisphere, for both tritons and α particles. Therefore only upper limits for the cross sections can be inferred at these angles.

The angular distributions in Figs. 2–7 show a strong peaking at forward laboratory angles for both tritons and α particles, indicative of the presence of preequilibrium processes. The 72.8 MeV data are similar, in both shape and magnitude, to those at 62.7 MeV.

The overall relative errors of the points in the energy spectra are about 7%, given by the accumulated statistics, except for lower energies, where they can be larger as a result of the procedure adopted for the thick target correction [1,16]. The uncertainty in the cross-section absolute scale is less than 10%, given by errors in the measured reference (n,p) cross sections (5%), beam monitoring (2%), statistics in the H(n,p) recoil proton peak (2%), and solid angle corrections (1%).

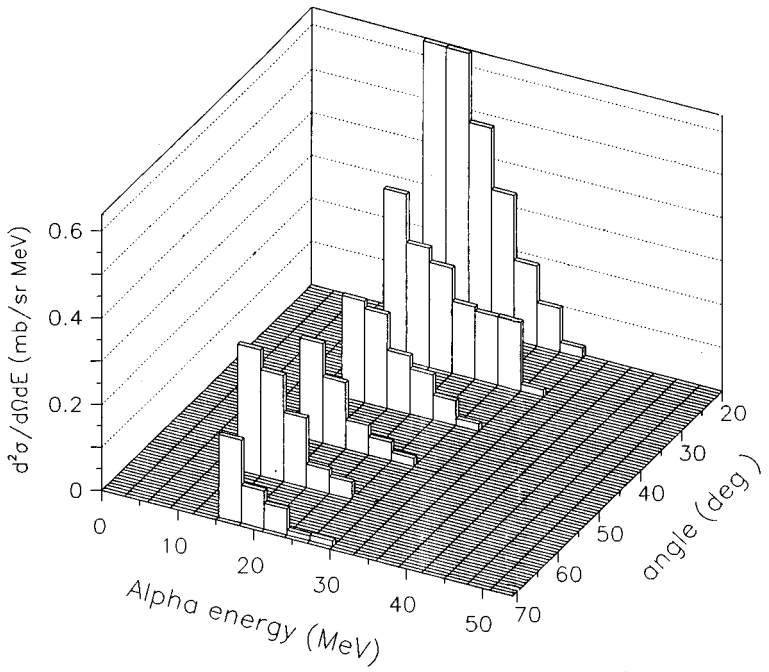

FIG. 3. Same as in Fig. 2 for the case of α particles.

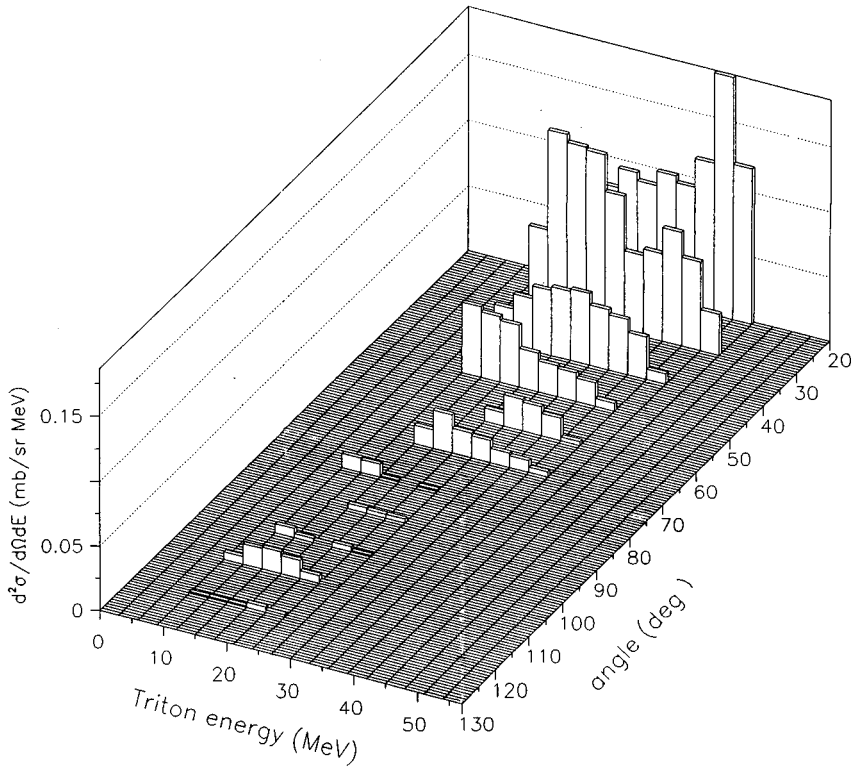

FIG. 4. Angular distributions of measured double-differential cross sections (histograms in steps of 3 MeV) for triton production at 62.7 MeV incident neutron energy.

IV. THEORETICAL MODEL

An accurate modeling of the interactions of fast neutrons with light nuclei presents a particular challenge for most nuclear reaction theories, since their derivations usually make use of statistical assumptions which are not valid when the density of nuclear states is low. With this cautionary comment, however, there are some reasons to suggest that the nuclear theories we use may provide a reasonable description of the measured spectra. First, as we discuss below, our calculations do include the low-lying (i.e., nonstatistical) energy levels of the nuclei involved in the reactions. Secondly, once the nuclear excitation energy exceeds approximately 10–15 MeV the density of states becomes relatively

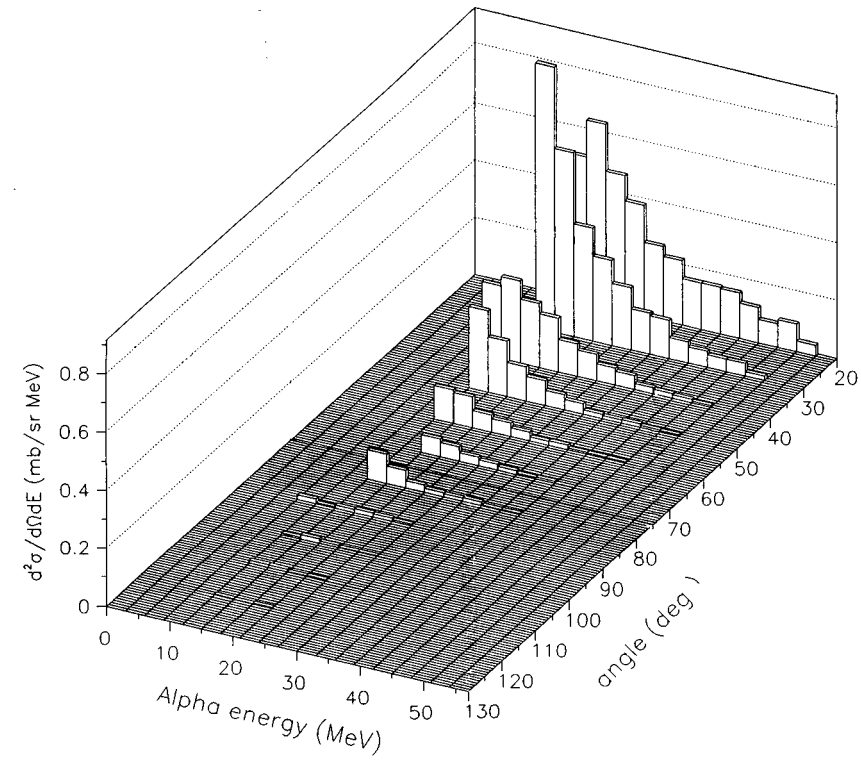

FIG. 5. Same as in Fig. 4 for the case of α particles.

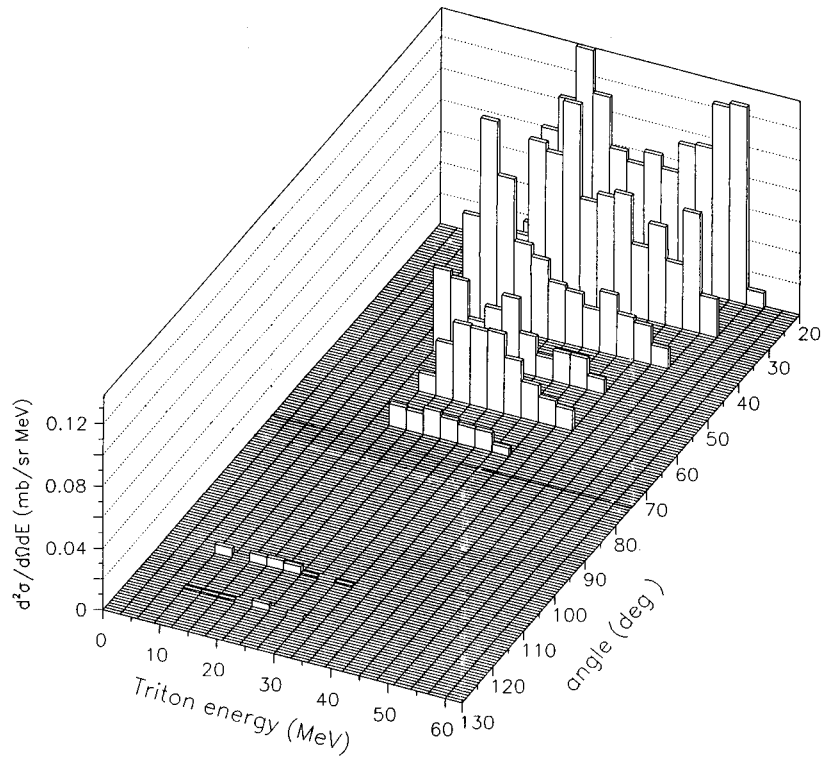

FIG. 6. Angular distributions of measured double-differential cross sections (histograms in steps of 3 MeV) for triton production at 72.8 MeV incident neutron energy.

large even for light nuclei, and statistical assumptions concerning the random phases of transition matrix elements would be expected to become valid. Finally, the measured angle-integrated emission spectra themselves generally show a reasonably smooth variation with emission energy except at the highest emission energies. In the present paper model calculations were performed with the FKK-GNASH code [17], which includes equilibrium, preequilibrium, and direct reaction mechanisms. The nuclear theories used to determine these emission cross sections are described below. Although we concentrate on the analysis of triton and α emission here, it is important also to accurately model the emission of neutrons, protons, deuterons, and γ rays, since these particles are emitted in competition and their cross sections influence

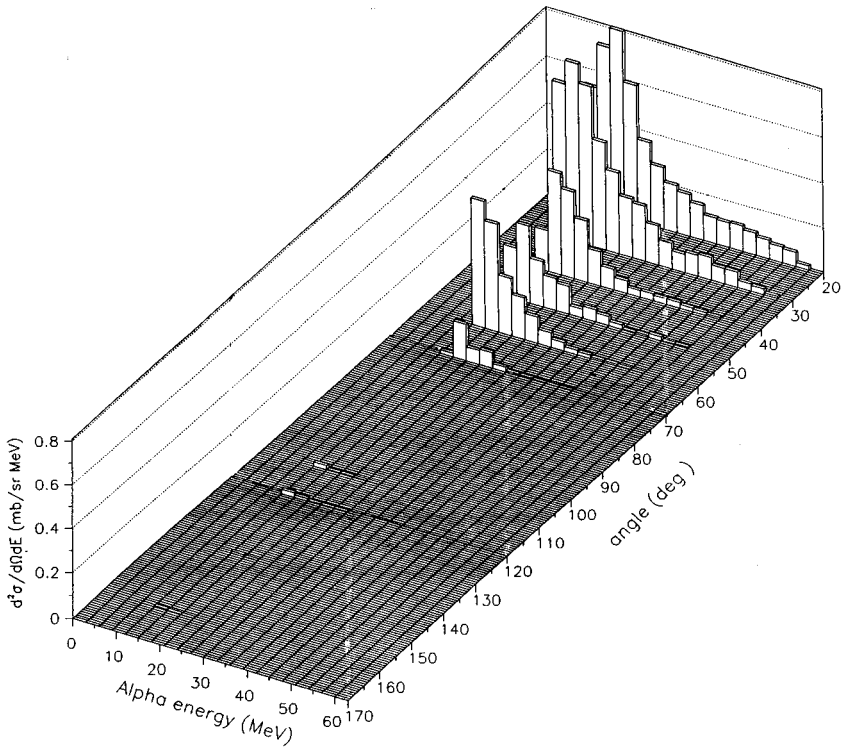

FIG. 7. Same as in Fig. 6 for the case of α particles.

those for triton and α emission. Our calculations describe the breakup processes in terms of two-body sequential decays. Thus, for example, the important $^{12}C(n,n'3\alpha)$ breakup channel is modeled as a sequence of two-body decays such as the $^{12}C(n,n')^{12}C^* \rightarrow \alpha + ^{8}Be^* \rightarrow 2\alpha$ process.

We used a coupled-channel optical model to describe direct inelastic and elastic neutron emission to low-lying states in carbon, with an externally input rotation-vibration form factor in the ECIS79 code [18]. This optical potential, with couplings between the 0^+, 2^+ (4.4 MeV), 4^+ (14.1 MeV), and 3^- (9.6 MeV) states, is based on the Ohio University potential developed by Meigooni *et al.* [19]. As shown in Ref. [20], it provides an excellent representation of total, nonelastic, and elastic cross sections, and elastic and inelastic angular distributions. In addition to neutron scattering, optical potentials for the other ejectiles are needed to generate transmission coefficients for the Hauser-Feshbach equilibrium emission calculations, and distorted wave functions for the preequilibrium nucleon emission calculations. For the proton optical potential we use the above neutron potential, with a Coulomb correction to the real central potential of $0.4Z/A^{1/3}$ (since $N=Z$ for carbon, no isospin transformation is needed). This potential gives a good description of proton elastic and inelastic angular distributions [19,21]. Potentials for deuterons, α particles and tritons were obtained using the method of Watanabe, as implemented by Madland [22].

The quantum mechanical Feshback-Kerman-Koonin (FKK) theory [23] is applied to describe preequilibrium nucleon emission. This theory pictures the nuclear reaction as passing through a series of preequilibrium particle-hole states towards equilibrium, as nucleon-nucleon collisions share the projectile's energy among the target nucleons. Two types of preequilibrium processes are distinguished: multistep direct (where at least one particle remains in the continuum, resulting in forward-peaked angular distributions), and multistep compound (where the excited particles remain bound, resulting in angular distributions symmetric about 90° in the center of mass). At the energies of interest in this work the multistep direct mechanism dominates, and these processes are determined by extending one-step distorted-wave Born approximation (DWBA) into the continuum, with multistep processes being obtained from a convolution of one-step scatterings. Full details of the formulas we used and the calculational procedures employed (including the coupling of multistep direct and compound preequilibrium chains) are given in Ref. [24].

While some progress has been made in formulating cluster-particle preequilibrium emission within the FKK theory [25], these calculations are still at an early stage of development. Therefore Kalbach's cluster exciton model was used to describe preequilibrium α, deuteron, and triton emission [26]. Modeling preequilibrium emission of composite particles is notoriously difficult, since quantities such as the extent of clustering in the target nucleus, the probabilities of nucleons forming a cluster during the preequilibrium cascade, and the interaction between clusters and nucleons influence the emission cross sections. As we shall show in the next section, the α spectra predicted by the exciton model agree fairly well with the measurements, though the agreement with the triton spectra is poorer.

Above about 50 MeV incident energy, multiple preequilibrium emission (where more than one fast preequilibrium particle is emitted prior to equilibration) becomes important, and we include these processes according to the theory of Ref. [27]. Since the emission of two fast nucleons prohibits subsequent 3α decay, we found that including multiple preequilibrium emission is important for accurately predicting α-particle production as well as inclusive nucleon emission spectra.

After preequilibrium particle emission has occurred, the equilibrated residual nuclei decay by particle or γ-ray emission. The Hauser-Feshbach theory was used to calculate these processes, including full angular momentum and parity conservation. We explicitly calculate the decay of carbon isotopes from ^{13}C to ^{9}C, boron isotopes from ^{12}B to ^{8}B, beryllium isotopes from ^{11}Be to ^{7}Be, lithium isotopes from ^{8}Li to ^{5}Li, and helium isotopes from ^{7}He to ^{5}He. Transmission coefficients for particle emission are obtained from the above optical potentials, and for γ-ray emission from the generalized Lorentzian model of Kopecky and Uhl [28] (which modifies the Brink-Axel hypothesis to include an energy-dependent giant resonance width from Fermi-liquid theory) for $E1$, $E2$, and $M1$ radiation. The inverse cross section for photoabsorption was taken from the measurement of Ahrens *et al.* [29].

Level densities for excited states were obtained by match-

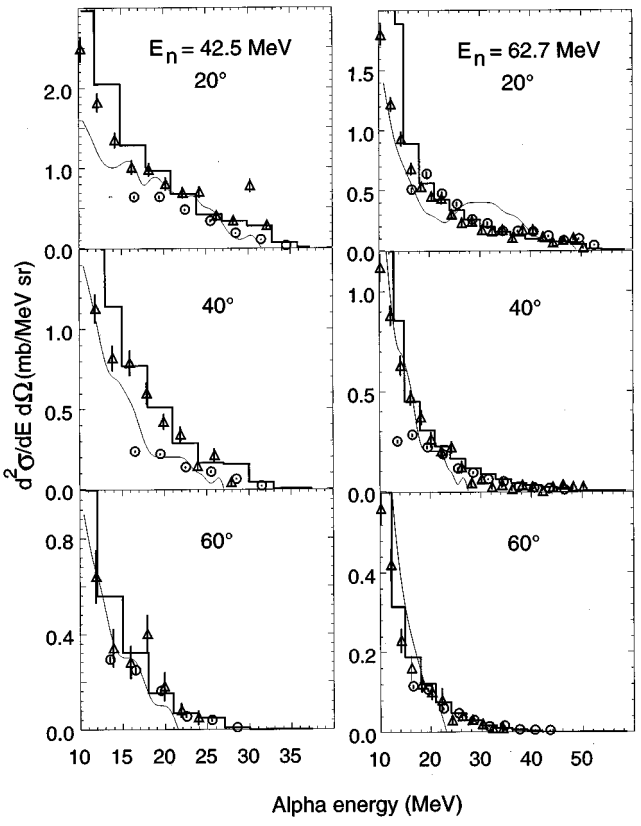

FIG. 8. Measured double-differential cross sections at several laboratory angles (open dots) for $^{12}C(n,\alpha x)$ reactions for 42.5 and 62.7 MeV incident neutron energies, respectively. Continuous line histograms are theoretical calculations of the present work. Experimental results of Ref. [3] at 39.7 and 60.7 MeV are shown as open triangles. Calculations for 40 and 60 MeV neutron energies from Ref. [6] are shown as continuous lines.

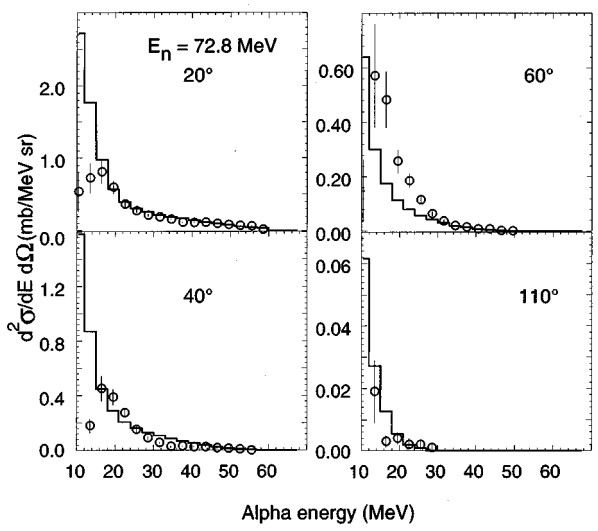

FIG. 9. Measured double-differential cross sections at several laboratory angles (open dots) for $^{12}C(n,\alpha x)$ reactions at 72.8 MeV incident neutron energy. Continuous line histograms are theoretical calculations of the present work.

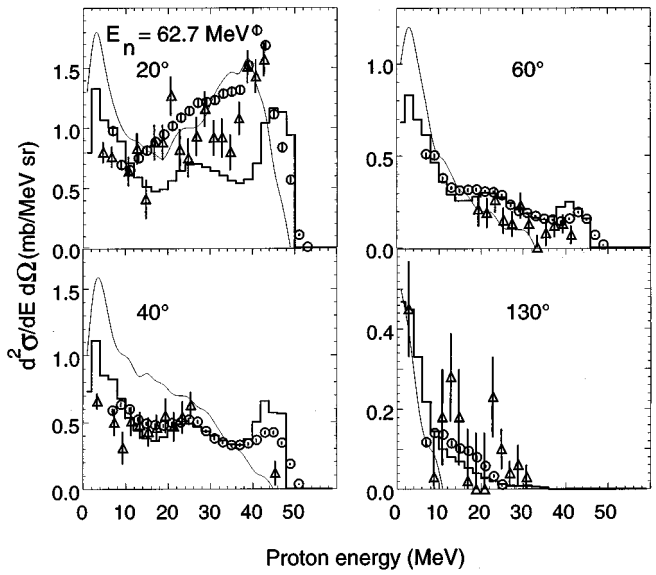

FIG. 11. Measured double-differential cross sections at several laboratory angles (open dots) for the $^{12}C(n,px)$ reactions at 62.7 MeV incident neutron energy [1]. Continuous line histograms are theoretical calculations of the present work. Experimental results of Ref. [3] at 60.7 MeV are shown as open triangles. Calculations at 60 MeV neutron energy from Ref. [6] are shown as continuous lines.

ing continuously the continuum statistical level density model of Ignatyuk, Smirenkin, and Tishin [30] (which includes a washing out of shell effects with increasing excitation energy) onto the measured discrete low-lying levels at lower excitation energies. Pairing energies were taken from the systematic of Cook with the Los Alamos extensions to light nuclei from Ref. [31]. For each residual nucleus that can be produced, we plot the cumulative number of measured discrete low-lying levels, taken from the Ajzenberg-Selove [32] compilations, against excitation energy, to determine the energy above which the statistical model can be used. Therefore, our calculations incorporate nonstatistical features of nuclei by explicitly including their discrete level energies, spins, and parities, up to a certain excitation energy (typically of about 10 MeV). Exact nuclear masses are used to determine particle separation energies so that energy conservation is fulfilled at each stage in the sequential decays.

Angular distributions for continuum particle emission were obtained by using the phenomenological systematics of Kalbach [33], which use a symmetric-about-90° distribution for equilibrium ejectiles, and a forward-peaked angular distribution for the preequilibrium ejectiles. Recently a physical basis for these systematics, which represent the multistep direct angular distributions in terms of an exponential in $\cos\theta$, has been presented [34]. The double-differential emission spectra are first obtained in the channel energy frame (the center of mass of the ejectile and residual nucleus), and are subsequently transformed into the laboratory frame using two-body kinematics. For a target nucleus as light as carbon the effect of this transformation on the spectra is large, and while our assumption of two-body kinematics breaks down at low emission energies, we expect that the errors introduced are small.

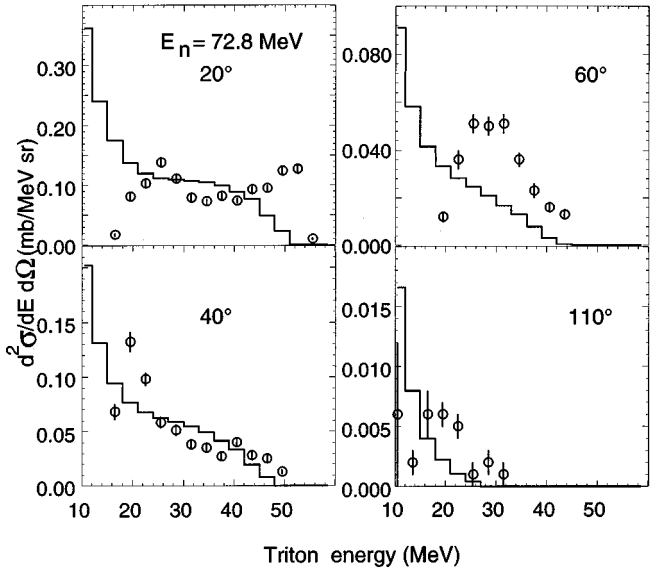

FIG. 10. Same as in Fig. 9 for the case of $^{12}C(n,tx)$ reactions.

V. COMPARISON BETWEEN EXPERIMENT AND THEORY

The cross sections in Figs. 2–7 can be compared with the UC Davis data from Ref. [3] and the results from model calculations. Figures 8–10 show double-differential cross sections for $^{12}C(n,\alpha x)$ and $^{12}C(n,tx)$, in 3 MeV energy bins, at several laboratory angles and incident neutron energies (note the change of scale from one angle to another). The experimental data of Ref. [3], shown as open triangles, are seen to be rather consistent with our measurements. Calculations using the theories in the FKK-GNASH code are shown

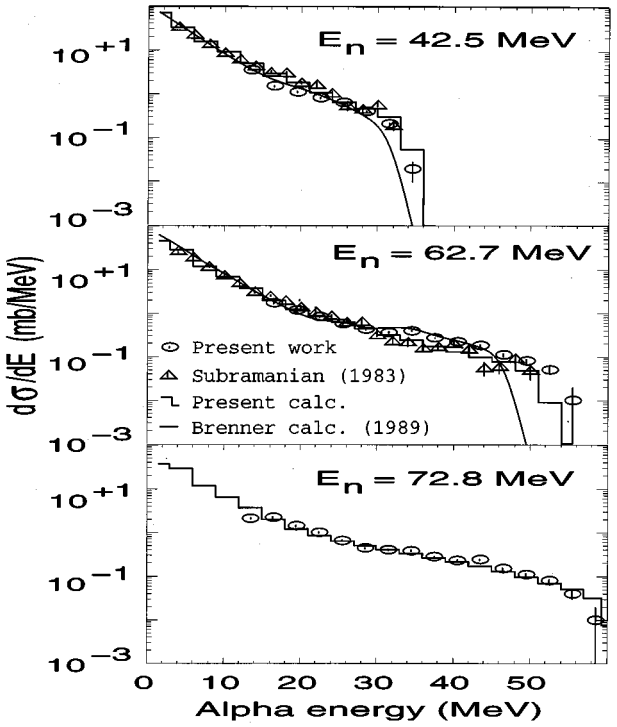

FIG. 12. Laboratory frame experimental energy-differential cross sections (open dots) for α production at the three incident neutron energies. Full line histograms are the corresponding model calculations of the present work. The open triangles are experimental results of Ref. [3] at 39.7 and 60.7 MeV. The continuous lines show the model calculations of Ref. [6] at 40 and 60 MeV incident neutron energies.

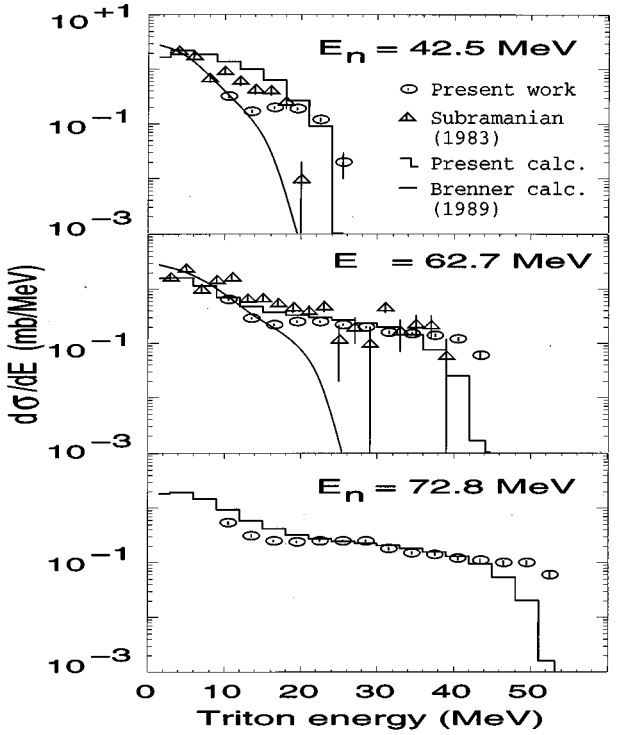

FIG. 13. Same as in Fig. 12 for the case of $^{12}C(n,tx)$ reactions.

as solid histogram lines, and the calculations of Brenner and Prael [6] using the intranuclear cascade code INCA (which includes α clustering and particle pickup, followed by Fermi breakup), are shown as continuous lines. It is worth mentioning that no supplementary normalization was used in Figs. 8–10 between theory and our experimental cross sections.

The $^{12}C(n,\alpha x)$ cross sections at 42.5 and 62.7 MeV are shown in Fig. 8, for laboratory angles of 20°, 40°, and 60°. The overall agreement between the calculations and the experimental data is seen to be rather good, for both the shape and the magnitude of the cross sections. The Brenner and Prael calculations [6] though, appear to underpredict the data at the higher emission energies, for the larger angles. At 72.8 MeV there are no other experimental or theoretical results to be compared with our data. In Fig. 9 our calculations again describe the 72.8 MeV measured $^{12}C(n,\alpha x)$ spectra fairly well. Figure 10 compares the experimental triton spectra at 72.8 MeV with our theoretical cross sections. Agreement between theory and measurement is poorer here, especially at 20° and 60°. Nevertheless, these cross sections are very small, and as discussed in Sec. IV it is difficult to accurately model triton emission. The preequilibrium cluster emission model does account for the presence of high-energy tritons above the evaporation region but the details of the measured spectra are not well reproduced.

Although proton emission is not the main subject of this paper, Fig. 11 shows the calculated proton spectra at 63 MeV compared with our previous results [1], the UC Davis values [3], and Brenner and Prael's calculations at 60 MeV. Since the calculated proton cross sections influence the results for α and triton emission, it is important that these calculations should account for the measurements. The present calculations describe the data fairly well except at 20° where they underpredict the data (since the Kalbach angular distribution systematics cannot account for such a large increase in the cross sections at very forward angles). The Brenner and Prael calculations describe the data well at this angle, but agreement is poorer at the other angles.

Energy-differential cross sections (in the lab frame) are presented in Fig. 12 for α emission, and in Fig. 13 for triton emission, for the three incident neutron energies. They are obtained by a solid angle integration of the data shown in Figs. 2–7. Figures 12 and 13 show for comparison the corresponding experimental values of Ref. [3] for 39.7 and 60.7 MeV, and theoretical predictions from the FKK-GNASH code (histograms) and from Brenner and Prael (continuous lines).

TABLE I. Total cross sections for triton and α-particle production induced by neutrons of 42.5, 62.7, and 72.8 MeV on carbon. Uncertainties are discussed in the text. Theoretical values are also shown for comparison.

Neutron energy (MeV)	$\sigma(n,tx)$ expt. (mb)	$\sigma(n,tx)$ theory (mb)	$\sigma(n,\alpha x)$ expt. (mb)	$\sigma(n,\alpha x)$ theory (mb)
42.5	20.0±5.5	27.1	414.2±129.5	426.8
62.7	20.7±4.5	22.0	301.0± 87.2	300.4
72.8	24.4±5.6	26.9	266.9± 75.6	269.5

TABLE II. Integrated cross sections above the experimental threshold cutoff energy (E_{thresh}) for triton and α-particle production induced by neutrons of 42.5, 62.7, and 72.8 MeV on carbon. Theoretical values are also shown for comparison.

Neutron energy (MeV)	E_{thresh} (MeV)	$\sigma(n,tx)>E_{\text{thresh}}$ expt. (mb)	$\sigma(n,tx)>E_{\text{thresh}}$ theory (mb)	E_{thresh} (MeV)	$\sigma(n,\alpha x)>E_{\text{thresh}}$ expt. (mb)	$\sigma(n,\alpha x)>E_{\text{thresh}}$ theory (mb)
42.5	9.0	3.0±0.2	10.2	12.0	25.9±1.3	38.7
62.7	9.0	8.1±0.4	9.4	15.0	19.2±1.0	18.6
72.8	9.0	9.2±0.5	11.6	9.0	43.4±2.2	51.5

The model predictions of α emission agree well with the experimental data (some underprediction of the highest-energy particles by Brenner and Prael [6] is expected since their calculations correspond to slightly lower incident energies). In the case of triton emission (Fig. 13) the FKK-GNASH calculations describe the data reasonably well, though they overpredict the measurements at 42.5 MeV, and show a steeper variation with emission energy compared to the measurements at 72.8 MeV. The calculations of triton emission by Brenner and Prael significantly underpredict the cross sections at higher emission energies.

The cross sections for α emission at the lower emission energies are particularly high, and exceed the cross sections for other charged-particle ejectiles. This is because the tight binding of α particles results in a high probability of their production during the carbon fragmentation process. At the lower incident energies, decay through one of the many 3α reaction sequences is rather likely, resulting in a large α-particle production. At higher incident energies the 3α cross section becomes smaller as other channels open up, but the presence of α particles in these other channels is still significant. Both of the model calculations account for these large low-emission-energy α-production cross sections, in the present work using sequential Hauser-Feshbach theory, and in Brenner and Prael's calculations using Fermi breakup.

Table I gives total cross sections for triton and α-particle production, resulting from the integration of the energy-differential cross sections in Figs. 12 and 13. Below the experimental energy cutoffs, and for the energy spectra at laboratory angles where no significant statistics were accumulated in the measurement, the theoretical cross sections of the present work are used to extrapolate the measurements. We estimate the uncertainty on the theoretical extrapolations at low emission energies to be about 30%, obtained by comparing differences between the present calculations and those of Brenner and Prael. The errors shown in Table I for the deduced experimental total production cross sections include these uncertainties of the theoretical cross sections. Additionally, Table I shows our theoretical values for the total production cross sections. It should be noted that because of the high values of the energy cutoffs in the measurements, the theoretical corrections at low emission energies dominate the total cross sections (particularly for α particles), and hence good agreement between theory and extrapolated experimental results is to be expected. Table II contains a similar comparison of experiment and theory, though only for the energy regions measured in this experiment, above the detector energy cutoffs. The theoretical results are seen to agree fairly well with the measurements, except for triton emission at 42.5 MeV where the theory overpredicts the data.

VI. CONCLUSIONS

Triton and α-particle production energy spectra ($d^2\sigma/d\Omega\, dE$) resulting from the interaction of fast neutrons on carbon, are reported at three incident energies between 40 and 75 MeV. Measurements were performed with good statistics at the fast-neutron facility of the Louvain-la-Neuve Cyclotron, Belgium. Angular distributions were measured at laboratory angles between 20° and 160° (in steps of 10°) for 42.5, 62.7, and 72.8 MeV incident neutron energies. Energy spectra are reported mainly for forward angles and, due to the low statistics accumulated, only upper limits could be established for the double-differential cross sections at some of the angles in the backward hemisphere. Energy-differential cross sections are deduced from our measured double-differential cross sections. Overall, these data compare rather well with previously reported measurements from UC Davis [3]. However, our new results extend to a higher incident energy than those measured at UC Davis, and cover the angular range more completely.

Our calculations using preequilibrium and equilibrium emission theories generally describe the experimental data fairly well. They account for the large cross sections of low-energy α particles and the presence of high-energy particles from preequilibrium processes. Triton emission is predicted less accurately. The α emission model calculations of Brenner and Prael [6] describe the data with an accuracy comparable to that of the present calculations, though with poorer accuracy for triton emission since they largely underpredict the high-energy tritons. At the incident energies studied in this work the experimental data, like the earlier UC Davis data, generally do not show strong fluctuations with varying emission energy (when averaged over 3 MeV), suggesting the applicability of the statistical assumptions made in the theories we use. We therefore conclude that for these incident energies (above 40 MeV) statistical models can be applied in the analysis of neutron reactions on carbon, particularly for reactions leaving residual nuclei with excitation energies above about 10–15 MeV when the nuclear level density becomes sufficiently high.

A limitation of the present work is its application of the Kalbach cluster preequilibrium model which, although able to account for many features of the measured high-energy α and triton spectra, is somewhat phenomenological in nature. A high priority for future research is the development of a theory for preequilibrium cluster emission which is grounded

in a microscopic derivation. Some recent progress has been made in this direction, including theories based on coalescence models [35], and phase space models [36], but further progress is still needed to yield a theory possessing a high degree of *a priori* predictability.

Only illustrative examples of detailed experimental results have been presented here. Complete measured double-differential production cross sections may be obtained in numerical form from Dr. I. Slypen. A comprehensive and detailed description of the experiment, data reduction procedures, and experimental results has been reported in Ref. [37].

ACKNOWLEDGMENTS

We would like to thank the Louvain-la-Neuve Cyclotron staff for permanent assistance and the quality of the beam. One of us (M.B.C.) acknowledges helpful discussions with Dr. H. Barschall, Dr. M. Blann, Dr. P. DeLuca, Dr. R. Finlay, Dr. R. Haight, Dr. C. Hartmann-Siantar, Dr. A. Meigooni, Dr. R. M. White, and Dr. P. G. Young. We acknowledge support from the Institut Interuniversitaire des Sciences Nucléaires, Belgium, the European Economic Community (Contract No. F13P-93-0084-BE), and the U.S. Department of Energy by the Lawrence Livermore National Laboratory under Contract No. W-7405-ENG-48.

[1] I. Slypen, V. Corcalciuc, and J. P. Meulders, Phys. Rev. C **51**, 1303 (1995).
[2] T. S. Subramanian, J. L. Romero, and F. P. Brady, Nucl. Instrum. Methods **174**, 475 (1980).
[3] T. S. Subramanian, J. L. Romero, F. P. Brady, J. W. Watson, D. H. Fitzgerald, R. Garett, G. A. Needham, J. L. Ullmann, C. I. Zanelli, D. J. Brenner, and R. E. Prael, Phys. Rev. C **28**, 521 (1983).
[4] C. D. Bowman *et al.*, Nucl. Instrum. Methods Phys. Res. Sect. A **320**, 336 (1992).
[5] R. A. Cecil, B. D. Anderson, and R. Madey, Nucl. Instrum. Methods **161**, 439 (1979).
[6] D. J. Brenner and R. E. Prael, At. Data Nucl. Data Tables **41**, 71 (1989).
[7] A. Bol, P. Leleux, P. Lipnik, P. Macq, and A. Ninane, Nucl. Instrum. Methods Phys. Res. **214**, 169 (1983).
[8] C. Dupont, P. Leleux, P. Lipnik, P. Macq, and A. Ninane, Nucl. Instrum. Methods Phys. Res. Sect. A **256**, 169 (1983).
[9] C. Dupont, Ph.D. thesis, Université Catholique de Louvain, 1987 (unpublished).
[10] J. A. Jungerman, F. P. Brady, W. J. Knox, T. Montgomery, M. R. McGie, J. L. Romero, and Y. Ishizaki, Nucl. Instrum. Methods **94**, 421 (1971).
[11] D. Horn, C. G. Ball, A. Galindo-Uribarri, E. Hagberg, R. B. Walker, R. Laforest, and J. Pouliot, Nucl. Instrum. Methods Phys. Res. Sect. A **321**, 273 (1992).
[12] F. Benrachi, B. Chambon, B. Cheynis, D. Drain, C. Pastor, D. Seghier, K. Zaid, A. Giorni, D. Heuer, A. Llères, C. Morand, P. Stassi, and J. B. Viano, Nucl. Instrum. Methods Phys. Res. Sect. A **281**, 137 (1989).
[13] J. Alarja, A. Dauchy, A. Giorni, C. Morand, E. Pollaco, P. Stassi, R. Billery, B. Chambon, B. Cheynis, D. Drain, and C. Pastor, Nucl. Instrum. Methods Phys. Res. Sect. A **242**, 352 (1986).
[14] I. Slypen, V. Corcalciuc, A. Ninane, and J. P. Meulders, Nucl. Instrum. Methods Phys. Res. Sect. A **337**, 431 (1994).
[15] I. Slypen, V. Corcalciuc, and J. P. Meulders, Rom. J. Phys. **38**, 431 (1993).
[16] I. Slypen, V. Corcalciuc, and J. P. Meulders, Nucl. Instrum. Methods Phys. Res. Sect. B **88**, 275 (1994).
[17] P. G. Young, E. D. Arthur, and M. B. Chadwick, Los Alamos National Laboratory Report No. LA-MS-12343, 1992.
[18] J. Raynal, Computer Code ECIS79, International Center for Theoretical Physics, Trieste, 1971.
[19] A. S. Meigooni, R. W. Finlay, J. S. Petler, and J. P. Delaroche, Nucl. Phys. **A445**, 305 (1985).
[20] M. B. Chadwick, M. Blann, P. G. Young, and G. Reffo, in *Proceedings of the International Conference on Nuclear Data for Science and Technology*, Gatlinburg, Tennessee, 1994, edited by K. Dickens (American Nuclear Society, La Grange Park, 1994), p. 658.
[21] M. B. Chadwick, M. Blann, L. J. Cox, P. G. Young, and A. Meigooni, Lawrence Livermore National Laboratory Report No. UCRL-ID-120829, 1995.
[22] D. G. Madland, in Proceedings of a Specialists' Meeting on Preequilibrium Reactions, Semmering, Austria, 1988, edited by B. Strohmaier, Nuclear Energy Agency of the OECD Report No. NEANDC-245, 1988, p. 103.
[23] H. Feshbach, A. Kerman, and A. Koonin, Ann. Phys. (N.Y.) **125**, 429 (1980).
[24] M. B. Chadwick and P. G. Young, Phys. Rev. C **47**, 2225 (1993).
[25] H. B. Olinayi, P. Demetriou, and P. E. Hodgson, J. Phys. G **21**, 361 (1995).
[26] C. Kalbach, Z. Phys. A **283**, 401 (1977).
[27] M. B. Chadwick, P. G. Young, D. C. George, and Y. Watanabe, Phys. Rev. C **50**, 996 (1994).
[28] J. Kopecky and M. Uhl, Phys. Rev. C **41**, 1941 (1990).
[29] J. Ahrens *et al.*, Nucl. Phys. **A251**, 479 (1975).
[30] A. V. Ignatyuk, G. N. Smirenkin, and A. S. Tishin, Sov. J. Nucl. Phys. **21**, 255 (1975).
[31] E. D. Arthur, Los Alamos National Laboratory Progress Report No. LA-9841-PR, 1983.
[32] F. Ajzenberg-Selove, Nucl. Phys. **A490**, 1 (1988); **A506**, 1 (1990).
[33] C. Kalbach, Phys. Rev. C **37**, 2350 (1988).
[34] M. B. Chadwick and P. Oblozinsky, Phys. Rev. C **50**, 2490 (1994).
[35] M. Cavinato, E. Fabrici, E. Gadioli, E. Gadioli Erba, M. Galmarini, and A. Gritti, Z. Phys. A **347**, 237 (1994).
[36] J. Bisplinghoff, Phys. Rev. C **50**, 1611 (1994).
[37] I. Slypen, Ph.D. thesis, Université Catholique de Louvain, 1995 (unpublished).